Using Sun Glint to Check the Relative Calibration of Reflected Spectral Radiances

GUNNAR LUDERER,* JAMES A. COAKLEY JR., AND WILLIAM R. TAHNK

College of Oceanic and Atmospheric Sciences, Oregon State University, Corvallis, Oregon

(Manuscript received 2 September 2004, in final form 28 January 2005)

ABSTRACT

Observations of sunlight reflected from regions of sun glint are used to check the relative calibration of spectral radiances obtained with imaging radiometers. Reflectances at different wavelengths for sun-glint regions are linearly related. Provided that the atmosphere is reasonably transparent at the wavelengths, the aerosol burden is reasonably light, 0.64-μm optical depth less than 0.2; the particles constituting the aerosol are reasonably large, as is the case for marine aerosols; and the solar zenith angle is less than about 35°, the linear relationships between reflectances at different wavelengths are rather insensitive to the factors that govern the reflectances themselves. The relationships are remarkably insensitive to atmospheric composition, surface wind speed and direction, illumination, and viewing geometry. The slopes and offsets of the linear relationships are used to assess the relative accuracies of the calibrations of the different channels. Such assessments would appear to be attractive for checks on the in-flight performance of aircraft-borne imaging radiometers. Here, observations of reflectances at 0.64, 0.84, 1.6, and 2.1 μm for regions of sun glint obtained with the *Terra* and *Aqua* Moderate Resolution Imaging Spectroradiometer (MODIS) instruments are shown to be consistent with each other. Observations of the 0.64- and 1.6-μm reflectances for the Tropical Rainfall Measuring Mission (TRMM) Visible and Infrared Scanner (VIRS) instrument are shown to be inconsistent with the MODIS observations, the VIRS 1.6-μm gain appearing to be too low by 9%. The 0.64-, 0.84-, and 1.6-μm reflectances obtained with the *NOAA-16* and *NOAA-17* Advanced Very High Resolution Radiometers (AVHRRs) for December 2002 are shown to be inconsistent with each other and inconsistent with the MODIS observations. Based on observations of the extensive ice sheets of Antarctica, the *NOAA-16* 0.64-μm gain is found to be too low by 5% and that for the 0.84-μm reflectance is too low by 12%; the *NOAA-17* 0.64-μm gain is found to be accurate (within 2%), but the 0.84-μm gain is too low by 15%. With the gains adjusted, the 0.64- and 0.84-μm reflectances obtained for regions of sun glint with the AVHRRs are consistent with each other and consistent with the *Terra* and *Aqua* MODIS observations. These results suggest that the gain for the *NOAA-16* AVHRR 1.6-μm reflectance is accurate (within 1%) and that for the *NOAA-17* AVHRR is too low by 5%. All of the observations were made with the AVHRR in the low-reflectance (high gain) mode. The accuracy of these assessments is expected to be about 5%.

1. Introduction

Maintaining the calibration of aircraft-borne radiometers used to measure reflected sunlight is a challenge. At best, radiometers can be calibrated in the field using an integrating sphere and a light source as has been done for the Moderate Resolution Imaging Spectroradiometer (MODIS) Airborne Simulator (MAS; King et al. 1996). But often calibration is performed in laboratories, sometimes months after the fieldwork, as was the case of the Multichannel Cloud Radiometer (MCR), which flew on the C-130 during the Indian Ocean Experiment (INDOEX) (Liu et al. 2001, 2003). Whether calibrated in the field or in laboratories, there are typically no means for verifying the calibration of aircraft-borne radiometers while in flight and subject to the temperature, moisture, pressure, and other stresses of the flight environment (Platnick et al. 2000). Here we propose the use of reflected radiances observed when viewing sun glint off water surfaces as a means of checking the relative accuracies of radiances at different wavelengths. In the procedure described here, if the accuracy of reflected radiances at one wavelength is known, observations of sun glint can be used to check the accuracies of the radiances at other wavelengths.

* Current affiliation: Department of Biogeochemistry, Max Planck Institute for Chemistry, Mainz, Germany.

Corresponding author address: J. A. Coakley Jr., College of Oceanic and Atmospheric Sciences, 104 COAS Admin. Bldg., Oregon State University, Corvallis, OR 97331-5503.
E-mail: coakley@coas.oregonstate.edu

Observations of cloud-free scenes containing sun glint from water surfaces reveal that reflectances at different wavelengths are linearly related. A Monte Carlo radiative transfer model was developed to study the sensitivity of the linear relationships to factors that affect the reflected radiances themselves, such as surface wind speed and direction, atmospheric composition, and sun–surface–sensor geometry. The results of the model indicated that for solar zenith angles less than about 35°, as long as the atmosphere is relatively transparent, the aerosol burdens are reasonably light, and the aerosol is made up of large particles (conditions to be discussed in more detail in the next section), the linear relationships among the reflected radiances prove to be rather insensitive to the features of the glint pattern, which depend on wind speed, wind direction, illumination, and viewing geometry. Consequently, if the accuracy of reflected radiances measured by an instrument at one wavelength is known, then observations of sun glint can be used to assess the accuracies of reflected radiances at other wavelengths. Even if the accuracies of reflected radiances for all channels are unknown, observations of sun glint for the conditions noted earlier can be used to check the relative accuracy of their calibrations.

The possibility of using observations of sun glint to transfer the calibration of reflected radiances at one wavelength to those at other wavelengths was recognized by Kaufman and Holben (1993). They noted that the ratio of the reflectances for regions in sun glint is insensitive to surface wind speed. They developed a method of using pristine ocean scenes viewed away from sun glint as calibration targets to obtain absolute calibrations for visible reflectances, those strongly affected by Rayleigh scattering, and then using the ratios of reflectances in regions of sun glint to transfer the calibration of the visible reflectances to near-infrared reflectances. Vermote and Kaufman (1995) improved upon this approach by using optically thick clouds with tops near the tropopause to transfer the dark ocean calibrations of visible reflectances to near infrared reflectances at wavelengths less than 1 μm. Optically thick, high-level clouds have reflectances that are independent of wavelength across the visible and near-infrared spectrum up to wavelengths of about 1 μm. At longer wavelengths variations in cloud particle sizes give rise to significant variations in the near-infrared reflectances.

Here the constancy of the reflectance ratios for regions of sun glint is demonstrated using MODIS reflectances at 0.64, 0.84, 1.6, and 2.1 μm. These channels are of interest because of their use in deriving aerosol and cloud properties (King et al. 2003). Observations are taken from both *Terra* and *Aqua*. Similar analyses are performed for the reflectances at 0.64 and 1.6 μm obtained with the Visible and Infrared Scanner (VIRS), which flew on the *Tropical Rainfall Measuring Mission* (*TRMM*) satellite, and for the reflectances at 0.64, 0.84, and 1.6 μm obtained with the Advanced Very High Resolution Radiometers (AVHRRs) that flew on National Oceanic and Atmospheric Administration (NOAA) satellites *NOAA-16* and *NOAA-17*. The *Terra* and *Aqua* MODIS reflectances produced consistent ratios among the reflectances at the different wavelengths suggesting stable calibrations. The VIRS reflectances produced ratios that were inconsistent with the MODIS ratios. The ratios were also inconsistent with an assessment of the radiometric accuracies of the VIRS 0.64- and 1.6-μm reflectances performed by Minnis et al. (2002), but consistent with a later assessment performed by Lyu and Barnes (2003). The AVHRR reflectances produced ratios that were also inconsistent with the MODIS observations and inconsistent with each other. Following the procedures developed by Loeb (1997), new calibrations for the *NOAA-16* and *NOAA-17* AVHRR 0.64- and 0.84-μm reflectances were derived using spatially uniform scenes of extensive Antarctic ice sheets. With the ice-sheet calibrations, the *NOAA-16* and *NOAA-17* AVHRR observations of sun glint at 0.64 and 0.84 μm were consistent with each other and with the observations of the *Terra* and *Aqua* MODIS instruments. For *NOAA-16*, the ice-sheet calibrations of the 0.64- and 0.84-μm reflectances were in reasonable agreement with earlier findings by Heidinger et al. (2002) and the reflectance ratios for sun glint indicated that the *NOAA-16* 1.6-μm reflectances obtained using the calibration coefficients proposed by Heidinger et al. agreed reasonably well with their assessment of the accuracy.

2. Theory and data analysis

Figure 1 illustrates the methods used to observe oceanic regions that contain sun glint and to assess the relative accuracy of the reflected radiances at different wavelengths. The figure shows an image created from 3.7-μm radiances obtained with MODIS on *Aqua*. The spatial resolution at nadir is 1 km. The dark background region is the cloud-free ocean region away from sun glint. The light background region is the sun-glint region. The rectangular box in the image indicates the portion of the data analyzed to establish the relationships among the reflectances and radiances for the different wavelengths. The boxed region is approximately 290 km in length and 12 km in width. The size of the region analyzed is not fixed. In each case, a region is chosen that appears to be free of clouds and spans a

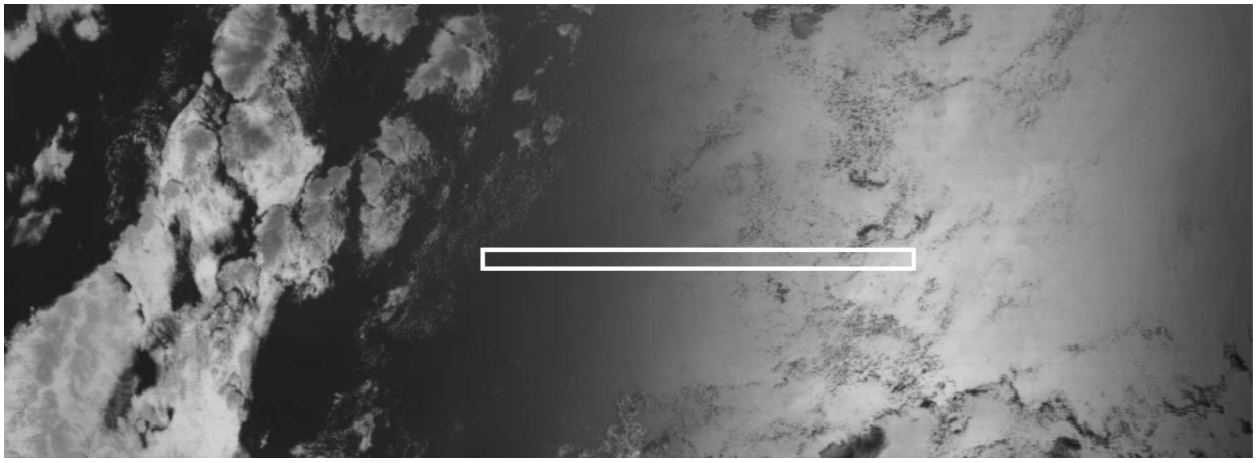

FIG. 1. Image of sun glint constructed from 1-km radiances at 3.7 μm. The data shown in Fig. 2 are from the boxed region. The boxed region is approximately 290 km in length and 12 km in width. The clouds in the image are low-level marine stratus. They appear as light objects against a dark background away from the sun glint and as dark objects against a light background in the sun glint. The observations are for *Aqua* on 8 Dec 2002 over the southern Indian Ocean at 0700 UTC.

major fraction of the sun glint, going from the edge to the center. To avoid clouds, the selected regions are often narrow, typically of order 10 km in width. The length of the region is selected to ensure good dynamic range in the reflectances. A rule of thumb is to select regions for which the largest reflectances at a particular wavelength are at least 3 times the smallest reflectances.

Relationships between the reflectances and radiances for the boxed region in Fig. 1 are plotted in Fig. 2. Ideally, the regions containing sun glint used in the analysis are cloud free. Clouds are avoided because reflected radiances in the near infrared are sensitive to cloud droplet size and droplet size varies from pixel to pixel at the 1-km scale of the satellite imagers. Here some cloud contamination is included in the region, in part to 1) illustrate the method used for cloud screening; 2) illustrate the effect of scattering and absorption in the atmosphere on the reflectances, both inside and outside of the region of sun glint; and 3) illustrate the effect of cloud contamination on the estimates of the slopes and intercepts for the reflectance relationships. The slopes and intercepts are used to determine the relative accuracies of the radiances.

The absolute radiances for the sun-glint region depend on the wind field, atmospheric composition, and the illumination and viewing geometry. The magnitude and direction of the surface wind determine the alignment and width of the distribution of slopes for the reflecting surfaces (Cox and Munk 1954). The distribu-

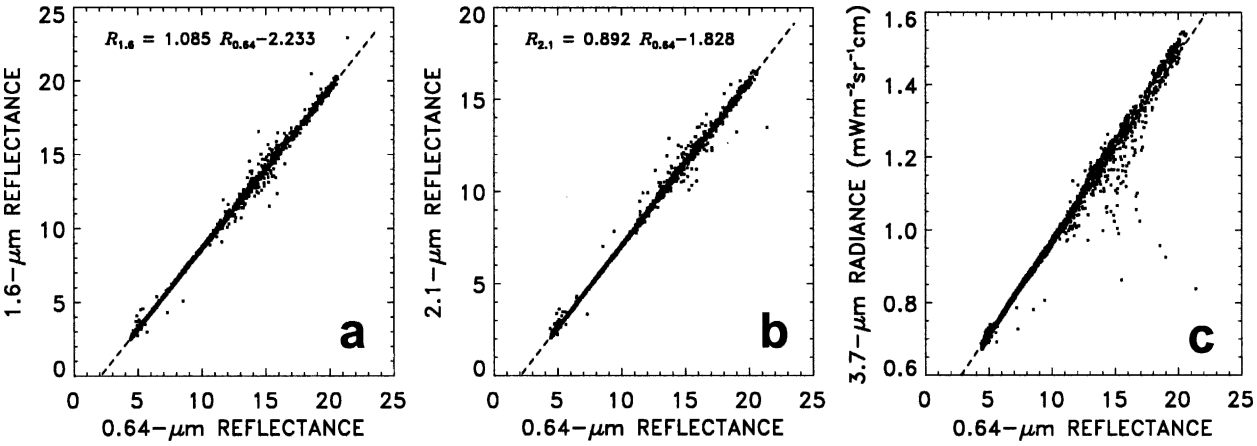

FIG. 2. The 1-km reflectances at 0.64, 1.6, and 2.1 μm, and radiances at 3.7 μm for the boxed region in Fig. 1. Dashed lines show linear least squares fits to the reflectances and radiances. The 3.7-μm radiances are used to detect significant cloud contamination in the sun glint. The 3.7-μm radiances falling below the fit line are due to cloud contamination.

tion of slopes in turn affects the bidirectional reflectance distribution function. To first order, in the sun glint, gaseous and aerosol extinction attenuate the reflected sunlight. Away from the glint region, scattering by aerosols enhances the reflected sunlight. Typically, there is insufficient information on atmospheric composition, aerosol properties, and surface winds to accurately calculate reflectances in the region of sun glint. On the other hand, as the distribution of the slopes for the reflecting surfaces is the same for all wavelengths, the linear relationship between reflectances at different wavelengths becomes insensitive to wind speed and direction. In fact, if the atmosphere were not present, the reflectances would be given by the product of the Fresnel reflectances multiplied by the probability distribution function for the surface slopes that allow the instrument to receive the specular reflection from the sun. The ratio of these reflectances at two wavelengths becomes the ratio of the Fresnel reflectances. The ratio is independent of wind speed and is nearly constant for solar zenith angles less than about 35°. With the atmosphere present, the ratio is modified by the scattering and absorption by gases and aerosols as discussed below.

Figure 2 illustrates the relative constancy of the sunglint reflectance ratios for the scene shown in Fig. 1. The reflectances used in Fig. 2 are given by

$$R = \frac{r}{\mu_0}, \tag{1}$$

where r is the "reflectance" obtained from the MOD02 level-1 data product and μ_0 is the cosine of the solar zenith angle associated with the reflectance. The constancy of the reflectance ratios is manifested in the linear relationships among the 0.64-, 1.6-, and 2.1-μm reflectances. A linear relationship is also found for the 3.7-μm radiances and the 0.64-μm reflectances because the effects of thermal gradients on the emitted radiances at 3.7 μm are small compared with the range of values for the reflected sunlight. In this study, the relationship between the 0.64-μm reflectance and 3.7-μm radiance is used to identify regions of the sun glint that are cloud contaminated and thus unsuitable for assessments of the relative calibration. The points in Fig. 2c that fall well below the trend line are due to clouds. Similar scatter about the trend line appears in the relationships among the 0.64-, 1.6-, and 2.1-μm reflectances, but the scatter is small and relatively ineffective as an indicator of cloud contamination. The relatively large departures at 3.7 μm are due in part to the greater absorption by water at 3.7 μm and to the lower thermal emission from the clouds when compared with the thermal emission from the surface. In the case of the AVHRR, the instrument is designed to observe radiances at either 1.6 (daytime) or 3.7 μm (nighttime). For the AVHRR, cloud contamination in the region of sun glint is detected using the joint distribution of 0.64-μm reflectances and 11-μm radiances in a manner analogous to that shown in Fig. 2c. As will be discussed below, the slopes of the relationships between the reflectances will be used to assess the gains of the instrument at the different wavelengths. The scatter of the points about the well-populated trend lines suggests that as long as cloud contamination is kept to relatively small levels, it has little impact on the values derived for the slopes.

Absorption and scattering in the atmosphere affect the slope of the relationship between the reflectances in that the direct beam reflected at the ocean surface and detected at the sensor, either on board an aircraft or satellite, is given by the product of the bidirectional reflectance distribution function and the sun–surface–sensor atmospheric transmission. Since the surface slope distribution is equal for all wavelengths, the ratio of the reflectances observed at different wavelengths is approximately equal to the ratio of the products of the Fresnel reflectances and the atmospheric path transmittances. To first order, in the glint region the transmission attenuates the direct beam. In Fig. 1, the attenuation at 3.7 μm due to absorption by the thin and broken clouds in the glint is sufficient to make them appear as dark objects against a light background. The effect is similar to the mechanisms employed by Kaufman et al. (2002), who proposed using the attenuation of the sun glint to estimate absorption by aerosols. The reflectance observed away from the glint, by contrast, is determined by the backscattering of the ocean–atmosphere system. In Fig. 1, reflection at 3.7 μm by clouds, even clouds that are as thin and broken as those in the glint region, is sufficient to make the clouds appear as light objects against a dark ocean background.

Owing to the different contributions of diffuse radiation for the different wavelengths, an intercept is encountered in the linear relationships for the reflectances. Both the reflectance of the ocean surface and scattering in the atmosphere tend to decrease with wavelength. Consequently, when representing reflectances in the near IR as linear functions of the 0.64-μm reflectance, the intercept is negative as is illustrated by the results in Fig. 2.

The slope of the linear relationship between the reflectances is determined through linear regression of the reflectances within a narrow domain spanning regions from the center to the edge of the glint as illustrated in Figs. 1 and 2. With aerosols present, the dif-

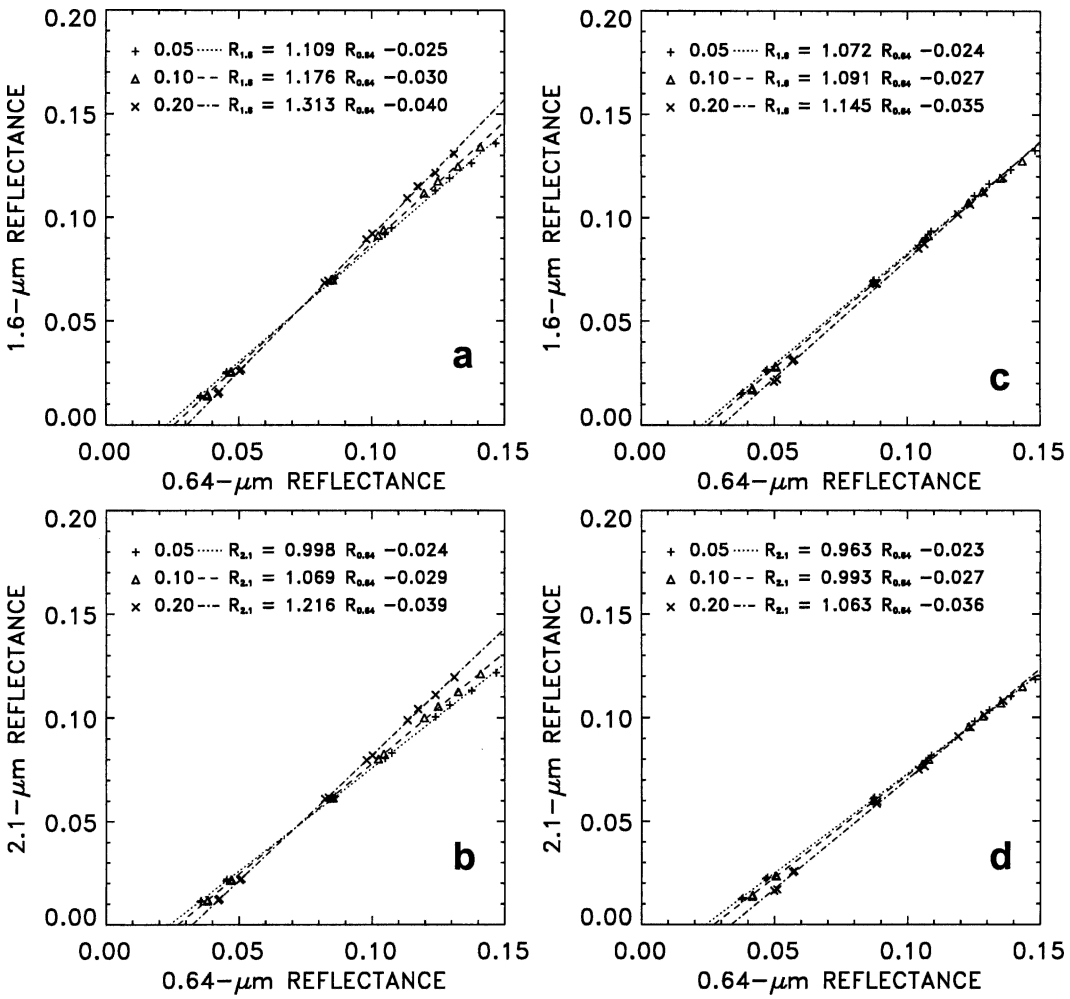

FIG. 3. The 0.64-, 1.6-, and 2.1-μm reflectances calculated using MOCARAT for three 0.64-μm optical depths, 0.05, 0.1, and 0.2, of (a), (b) average continental and (c), (d) tropical marine aerosols. All of the calculations were performed for a solar zenith angle of 22.5°. The symbols represent reflectances evaluated for the discrete satellite zenith and relative azimuth angles used in the calculations.

fuse reflection away from the sun glint increases due to increased backscattering, whereas the observed brightness in the center of the sun glint decreases due to the aerosol extinction. Large aerosol burdens therefore produce large slopes, the contrast between the in glint and away from glint reflectances at the reference wavelength, 0.64 μm, suffering greater reduction in comparison with reflectances at longer wavelengths. The strategy for obtaining relative calibrations among the channels is thus to seek regions with small aerosol burdens and in which the particles are large thus giving rise to reflectances that are much less sensitive to wavelength than is the case for aerosols with small particles. Fortunately, the southern Indian Ocean appears to be relatively aerosol free and the main component of the aerosol is sea salt, which has a relatively large particle size (Ramanathan et al. 2001; Coakley et al. 2002; Tahnk and Coakley 2002a).

To assess the sensitivity of the linear relationship for reflectances at various wavelengths, reflectances were simulated using a Monte Carlo Radiative Transfer (MOCARAT) model developed specifically for this purpose. MOCARAT employs a forward Monte Carlo technique for the computation of the reflectances observed over the atmosphere–ocean system. It accounts for gaseous absorption, Rayleigh and Mie scattering, and bidirectional reflection at the ocean–atmosphere interface. In the simulations, climatological tropical marine profiles were used for temperature and gaseous concentrations, particularly ozone and water vapor. Aerosol properties used in the simulations were taken from Hess et al. (1998). Figure 3 shows the sensitivity of

the linear relationships obtained for the simulated reflectances in the case of the Hess et al. (1998) average continental aerosol and tropical marine aerosol, both at a relative humidity of 80% and at three optical depths. The average continental aerosol absorbs sunlight and is composed of relatively small particles. The tropical marine aerosol is nonabsorbing and is composed of relatively large particles. The Ångström wavelength exponent between 0.64 and 1.64 μm is 1.6 for the average continental aerosol but only 0.2 for the tropical marine aerosol.

The numerical error in the modeled linear relationship that results from the use of the Monte Carlo technique and the discretization is smaller than 1% of the reflectances. The accuracy of the model is, however, limited by the validity of the assumed aerosol properties. Consequently, the overall error is expected to be significantly larger than the numerical error.

Figure 3 shows that for a solar zenith angle of 22.5° the slope for the 1.6–0.64-μm reflectances is 1.07 for a 0.64-μm optical depth of 0.05 and 1.14 for an optical depth of 0.2. For comparison, with an average continental aerosol in place of the marine aerosol the slope is 1.11 for an optical depth of 0.05 and 1.31 for an optical depth of 0.2. Owing to significant differences in extinction for the average continental aerosol at 0.64, 1.6, and 2.1 μm, the slopes of the linear relationships between the near IR and visible reflectances are relatively large and their sensitivity to aerosol burden is also relatively large. For the tropical marine aerosol, the differences between the aerosol extinctions in the visible and the near IR are relatively small. Consequently, the slopes of the linear relationships for the reflectances are smaller, and their sensitivity to aerosol burden is also significantly smaller. Values of the slopes and intercepts derived for simulations of the reflectances for atmospheres with marine aerosols reveal that they are rather insensitive to surface wind speed and direction, to aerosol burden, as long as the 0.64-μm optical depth is less than about 0.2, and to solar zenith angle, as long as the zenith angle is less than about 35°.

The slopes and intercepts of the linear relationships among the reflectances are used to assess, in a relative sense, the calibration of the radiometer. If the accuracy of radiances for a reference wavelength, here taken to be 0.64 μm, is known, then inferences can be made concerning the accuracies of radiances at the other wavelengths. Assume that the relationship between the actual reflectance R and the observed reflectance R' is given by

$$R = AR' + B, \tag{2}$$

where A and B are taken to be adjustments to the gain and offset of the instrument. From observations of the sun glint, the observed reflectance is related to the reference reflectance by

$$R' = S'R_{\mathrm{REF}} + C', \tag{3}$$

where the slope $S'$and intercept C' are determined from linear regression. Here the reflectance at the reference wavelength R_{REF} is assumed to be accurate. Algebraic manipulation of (2) and (3) leads to adjustments to the instrument gain and offset given by

$$A = \frac{S}{S'} \quad \text{and} \quad B = C - AC', \tag{4}$$

where values for S and C are expected values for the slope and intercept as might be obtained with a well-calibrated radiometer or from a model like MOCARAT. Uncertainties in the adjustments to the gains and offsets of the instrument are thus based on the accuracy of the calibrated reference radiometer or the model used to calculate the expected slopes and intercepts, the uncertainties of the slopes and intercepts derived from the observations and, of course, the accuracy of the radiances at the reference wavelength.

When using a model to derive the expected slopes and offsets, the largest source of uncertainty in (4) is the adequacy of the optical model for the aerosols. In the next section observations spanning more than a month are used to derive estimates of the slopes and intercepts. Owing to the period over which the observations are taken and the range of locations from which they are taken, a reasonable assumption is that the observations incorporate a range of aerosol burdens. Despite this range of aerosol burdens the uncertainty in the observed slopes is typically less than 3% and the uncertainty in the observed intercepts is typically 10%–20%. Consequently, the overall uncertainty in the adjustments to the gains, not allowing for uncertainties due to inaccurate reflectances at the reference wavelength, is probably less than 5% and thus typical of other methods used for the vicarious calibration of radiometers (Rao and Chen 1995; Heidinger et al. 2002). For the instrument offset, uncertainties in the slope and intercept of the reflectance relationship counter each other producing an uncertainty in the instrument offset that is relatively small. The effect of this offset is additive to the reflectances and as this additive component is typically small, the effect on the estimated reflectances is also relatively small, but may represent a sizable contribution for dark, cloud-free surfaces.

For aircraft-borne imaging radiometers, like MAS and the MCR, estimates of the gain could be even more accurate than those derived here for satellites. For the examples used here, the observations of sun glint typi-

cally cover hundreds of kilometers, as in Fig. 1, and thus are bound to include gradients in aerosol burdens. In addition, observations over a period of time, and in the cases studied here, for different locations, are bound to also include a range of aerosol properties. The range of aerosol properties leads to a range of values for the slopes derived for the reflectances at the different wavelengths. Observations from aircraft, on the other hand, are generally limited to regions of the order of tens of kilometers and a period of at most a few hours. Over such space and time scales, aerosol burdens are much more likely to be spatially and temporally uniform thereby limiting the range of the slopes derived for the reflectance relationships.

3. Results

The requirement that the aerosol burden be small and the aerosols be composed of large particles suggests that pristine oceans with marine aerosols are likely to provide the best targets. As noted earlier, observations in the southern Indian Ocean indicate that it may be an ideal target (Ramanathan et al. 2001). Observations of the southern Indian Ocean were collected for VIRS on *TRMM*, for AVHRR on *NOAA-16* and *NOAA-17*, and for MODIS on *Terra* and *Aqua*. To increase the intensity of the glint in the Southern Hemisphere, observations were collected for the austral summer, primarily December and January, although in the case of VIRS, the observations were for February and March. In the case of the *Terra* MODIS, observations of the sun glint were extracted from 37 passes over the southern Indian Ocean spanning the months of December 2001 and January 2002. For *Aqua*, the observations were extracted from 42 passes spanning the months of December 2002 and January 2003. The slopes and intercepts for *Terra* are shown in Fig. 4; those for *Aqua* are shown in Fig. 5. The results are summarized and compared with those of MOCARAT in Table 1.

The MODIS instruments produced consistent slopes and intercepts for the 0.64-, 1.6-, and 2.1-μm reflectances. Interestingly, in the case of the 0.64- and 1.6-μm reflectances, the slopes calculated with MOCARAT were within 1% of the observed slopes. Such agreement should be considered somewhat fortuitous as the offsets are clearly discrepant, and the slopes and offsets predicted for the 0.64- and 2.1-μm reflectances are likewise clearly discrepant. Based on the results shown in Fig. 3 and Table 1, it would appear that the calculated reflectances are more sensitive than the observed reflectances to the presence of aerosol at 0.64 and less sensitive at the near infrared wavelengths.

Not all of the variability in the slopes and intercepts

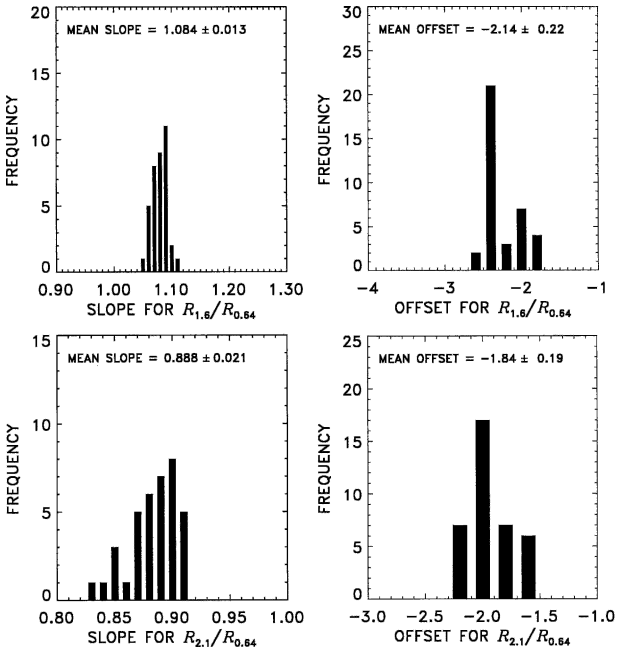

FIG. 4. Slopes and intercepts for the 0.64-, 1.6-, and 2.1-μm reflectances. The observations are from 37 passes of *Terra* over the southern Indian Ocean spanning Dec 2001 and Jan 2002. The values in the figures give the means and standard deviations of the slopes and intercepts.

can be attributed to changes in atmospheric composition, such as variations in ozone, water vapor concentrations, and especially aerosol burdens. The slopes and intercepts are also weakly dependent on solar zenith angle. Figure 6 shows the sensitivity of the slopes for the 0.64- and 1.6-μm relationship for the *Terra* and *Aqua* MODIS data. The sensitivity is given by the trend line, which in the figure is a linear least squares fit to the observations. Scatter about the trend line represents effects due primarily to the variability in aerosol properties. The sensitivity of the slope is relatively small, but the slope is a function of the solar zenith angle and this dependence in turn depends on the scattering and absorption in the atmosphere. The sensitivity of the slope for the 0.64–1.6-μm relationship is approximately 0.02 for a change in solar zenith angle from 20° to 30°. Similar sensitivities are found for the other sensors analyzed in this study. As indicated by the results in Table 1, the reflectance ratios simulated by MOCARAT exhibit a somewhat higher sensitivity to solar zenith angle.

Figure 7 shows the slopes and intercepts for the relationship between the 1.6- and 0.64-μm reflectances obtained with VIRS. In this case, the observations are for 22 passes over the southern Indian Ocean spanning February and March 1998. For the VIRS instrument, reflected radiances were converted to reflectances us-

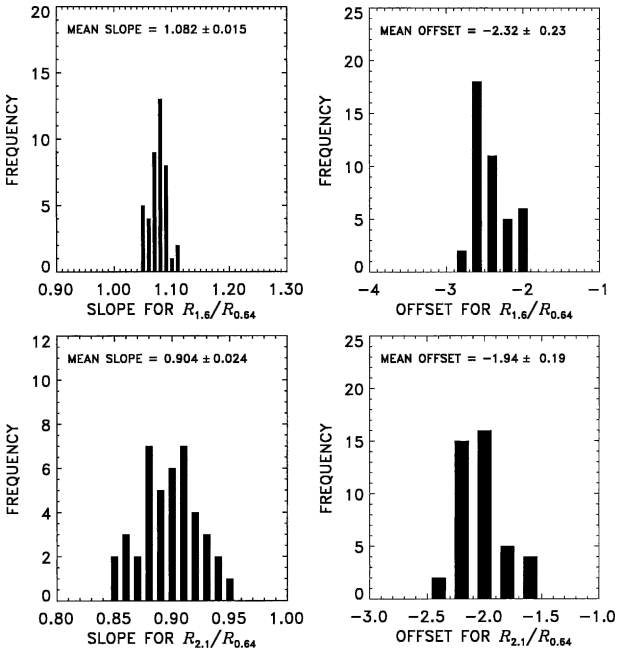

FIG. 5. Same as in Fig. 4 but from 42 passes of *Aqua* over the southern Indian Ocean spanning Dec 2002 and Jan 2003.

ing the solar constants for the spectral channels given by Lyu et al. (2000). The slope for the 1.6–0.64-μm reflectances is substantially smaller than the slopes obtained for both MODIS instruments. Because *TRMM* is in a non–sun synchronous orbit, the observations for VIRS include solar zenith angles ranging from 2.8° to 32.7° with an average of 21.6° The range is much greater than those for the MODIS observations as *Terra* and *Aqua* are in sun synchronous orbits. Nonetheless, the average of the solar zenith angles for the VIRS observations is near those for the MODIS observations and the dependence of the slope on solar zenith angle is sufficiently weak, like that shown for MODIS in Fig. 6, that the differences between the slopes cannot be explained by differences in solar zenith angles. Based on (4), assuming that the MODIS observations are accurate and that the 0.64-μm reflectance obtained with VIRS for February and March 1998 is accurate, which appears to be the case (Minnis et al. 2002; Lyu and Barnes 2003), the gain of the VIRS 1.6-μm channel appears to be too low by about 9%. This result is in close agreement with the 8.2% shortfall estimated by Lyu and Barnes (2003) and is clearly smaller than the 17% shortfall reported by Minnis et al. (2002).

Figure 8 shows the slopes and intercepts for the 1.6- and 0.64-μm relationship for the *NOAA-16* AVHRR. Figure 9 shows the slopes and intercepts for the *NOAA-17* AVHRR. Observations of the southern Indian Ocean were taken from 50 passes of *NOAA-16* and from 77 passes of *NOAA-17*. The observations for both satellites spanned December 2002. With the exception of the 1.6-μm channel of the *NOAA-16* AVHRR, the results shown in Figs. 8 and 9 were calibrated using the prelaunch calibration coefficients which are present in the level 1B data stream. NOAA has updated the calibration coefficients for the *NOAA-16* AVHRR data collected after May 2003 and for the *NOAA-17* AVHRR data collected after May 2004. In the case of the 1.6-μm channel of the *NOAA-16* AVHRR, Heidinger et al. (2002) noted that the prelaunch coefficients appeared to be in error. The coefficients produced a zero reflectance instrument space count (78) that was grossly inconsistent with the observed space count (approximately 40). Here, the coefficients for the 1.6-μm channel derived by Heidinger et al. (2002) are used instead of the prelaunch values. Heidinger et al. derived these coefficients by comparing *Terra* MODIS and *NOAA-16* AVHRR reflectances for two scenes of carefully collocated imagery, one scene taken from May and the other from July 2001. The results in Fig. 8 suggest that for the *NOAA-16* AVHRR the average slope for the 1.6- and 0.64-μm reflectances is somewhat larger than that for MODIS while for *NOAA-17* the average slope is somewhat smaller. If the

TABLE 1. Slopes and intercepts for the linear relationships between spectral reflectances.

		Solar zenith angle	1.6- and 0.64-μm reflectances		2.1- and 0.64-μm reflectances	
	Period	(°)	Slope	Intercept (%)	Slope	Intercept (%)
MODIS on *Terra*	Dec 2001–Jan 2002	21.2 ± 2.3	1.083 ± 0.012	−1.98 ± 0.17	0.888 ± 0.021	−1.71 ± 0.16
MOCARAT	—	21	1.093 ± 0.009	−2.76 ± 0.09	0.991 ± 0.005	−2.72 ± 0.05
MODIS on *Aqua*	Dec 2002–Jan 2003	23.6 ± 2.2	1.080 ± 0.013	−2.11 ± 0.16	0.903 ± 0.024	−1.77 ± 0.15
MOCARAT	—	24	1.096 ± 0.008	−2.76 ± 0.07	0.998 ± 0.005	−2.73 ± 0.05
VIRS	Feb–Mar 1998	21.6 ± 9.6	0.990 ± 0.029	−1.69 ± 0.34	—	—
AVHRR on *NOAA-16*	Dec 2002	30.1 ± 2.2	1.144 ± 0.026	−2.34 ± 0.25	—	—
MOCARAT	—	30	1.160 ± 0.009	−3.09 ± 0.09		
AVHRR on *NOAA-17*	Dec 2002	26.3 ± 2.2	1.030 ± 0.019	−2.09 ± 0.25	—	—
MOCARAT	—	26	1.124 ± 0.005	−2.94 ± 0.06	—	—

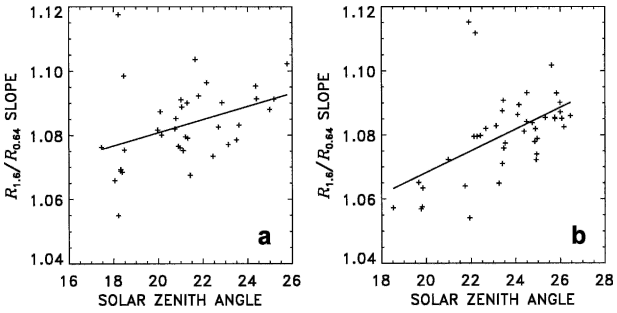

FIG. 6. Slopes and solar zenith angles for the 0.64- and 1.6-μm reflectances. The observations are from the (a) *Terra* passes of Dec 2001 and Jan 2002 and the (b) *Aqua* passes of Dec 2002 and Jan 2003.

reflectances at 0.64 μm are correct, which will be addressed in the next section, the gain of the *NOAA-16* AVHRR 1.6-μm channel is too large by (1.14/1.08 = 1.06) 6%, and that for the *NOAA-17* AVHRR 1.6-μm channel is too small by 5%. While the slopes for the *NOAA-16* and *NOAA-17* AVHRRs are separately close to the 5% accuracy expected for the sun-glint calibration check, the 11% discrepancy between the two instruments suggests that the radiometric calibration of these instruments might benefit from further study. In addition, the somewhat larger slope for the *NOAA-16* AVHRR 1.6-μm channel would appear to be inconsistent with the MODIS-AVHRR comparison reported by Heidinger et al. (2002) who found the 1.6-μm reflectances for the *NOAA-16* to be about 6% below those for the *Terra* MODIS. As will be shown in the next section, however, the *NOAA-16* 0.64-μm reflectances appear to be too low.

4. *NOAA-16* and *NOAA-17* 0.64- and 0.84-μm reflectances

Sunlight reflected from the sun-glint region is highly polarized. For the cross-track scanners and viewing geometries in this study, Fresnel reflection suggests that almost 80% of the reflected light is polarized with the polarization vector aligned parallel to the orbital direction. The departures of the results for the *NOAA-16* and *NOAA-17* AVHRRs from those for MODIS might result from differences in the sensitivities of the instruments to polarization. The prelaunch sensitivity of MODIS was found to be small, less than 1%–2% (X. Xiong, MCST, 2004, personal communication) and that found for the VIRS instrument was less than 5% (W. Barnes, NASA GSFC, 2004, personal communication). To test the possibility that the AVHRR reflectances showed significant sensitivity to polarization, observations of sun glint at 0.64 and 0.84 μm were compared for the MODIS and AVHRR instruments. In the case of the reflectances at 0.64 and 0.84 μm, references have been established for the spatially uniform portions of extensive Antarctic ice sheets (Loeb 1997). Unfortunately, owing to the sensitivity of reflectances at near infrared wavelengths to the size of ice grains, similar references cannot be derived for the 1.6- and 2.1-μm reflectances. Here the observations of sun glint at 0.64 and 0.84 μm are compared with those of spatially uniform regions of Antarctic ice to establish the consistency of these vicarious calibration methods. The comparisons also provide a measure of the possible impact

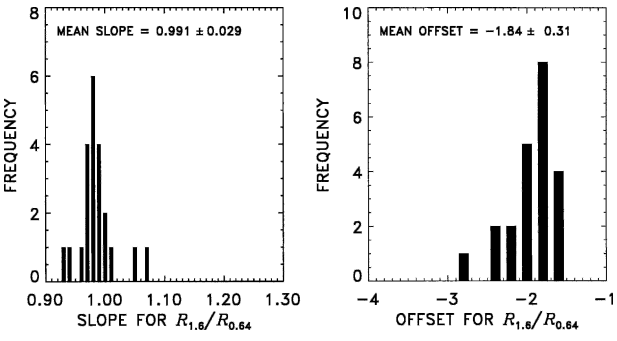

FIG. 7. Slopes and intercepts for VIRS 0.64- and 1.6-μm reflectances. The observations are from 22 passes of *TRMM* over the southern Indian Ocean spanning Feb and Mar 1998. The data are from the version 5 processing.

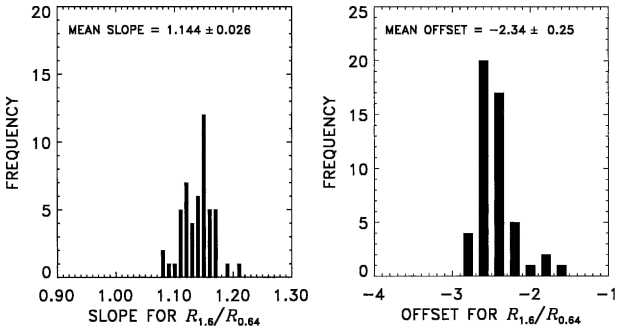

FIG. 8. Same as in Fig. 7 but for AVHRR from 50 passes of *NOAA-16* over the southern Indian Ocean for Dec 2002.

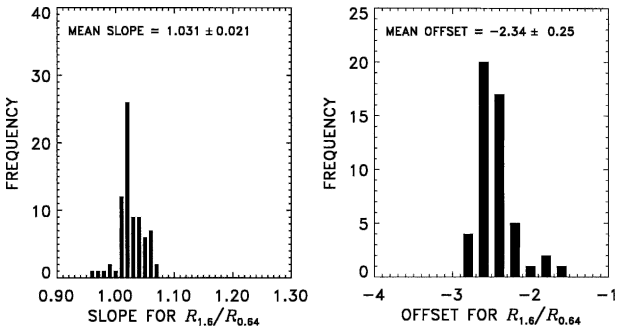

FIG. 9. Same as in Fig. 8 but from 77 passes of *NOAA-17* over the southern Indian Ocean for Dec 2002.

of polarization on the sun-glint observations, as the degree of polarization is much smaller for the observations of the ice sheets than for the observations of the sun glint.

Figure 10 shows the slopes and intercepts of the 0.64- and 0.84-μm reflectances observed with MODIS on *Terra* and *Aqua* for the sun-glint regions used to compile the results in the previous section. As with the 1.6- and 2.1-μm reflectances, the range of slopes and intercepts obtained for the MODIS observations are tightly clustered about mean values despite the range of aerosol burdens and locations observed. Also, the observations for the two MODIS instruments are consistent with each other.

Figure 11 shows the corresponding slopes and intercepts for the AVHRR on *NOAA-16* and *NOAA-17*. Here, the reflectances at 0.84 μm were divided by 0.82 to bring them into line with the MODIS observations. This correction is made to account for the effects of absorption by water vapor in the AVHRR channels that are absent in the MODIS channels. The correction is derived from the ratios of the 0.935- and 0.905-μm reflectances obtained from the MODIS on *Aqua* for a sample of the regions observed with the AVHRRs. The reflectance ratio $R_{0.935}/R_{0.905}$ is a measure of the column water vapor burden (Gao and Goetz 1990). The correction used here is derived from the $R_{0.935}/R_{0.905}$ ratios using results presented by Heidinger et al. (2002, their Fig. 6). The observed ratios indicate that the correction

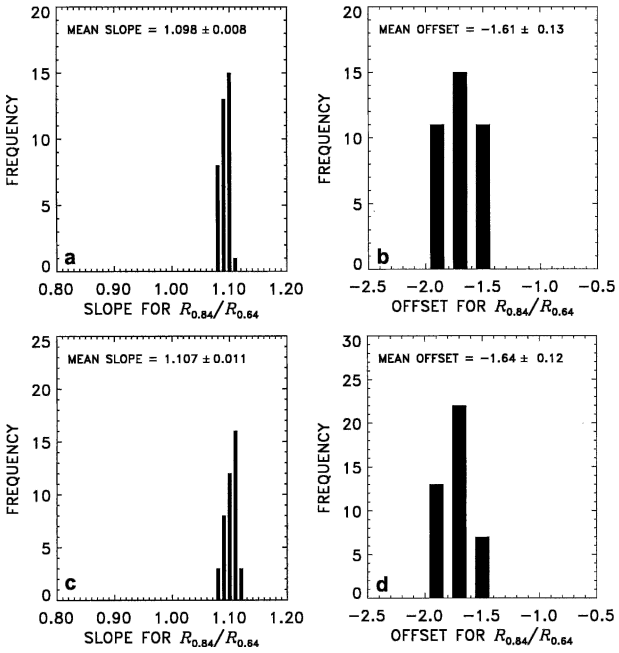

FIG. 10. Slopes and intercepts for MODIS 0.64- and 0.84-μm reflectances from (a), (b) *Terra* and (c), (d) *Aqua*.

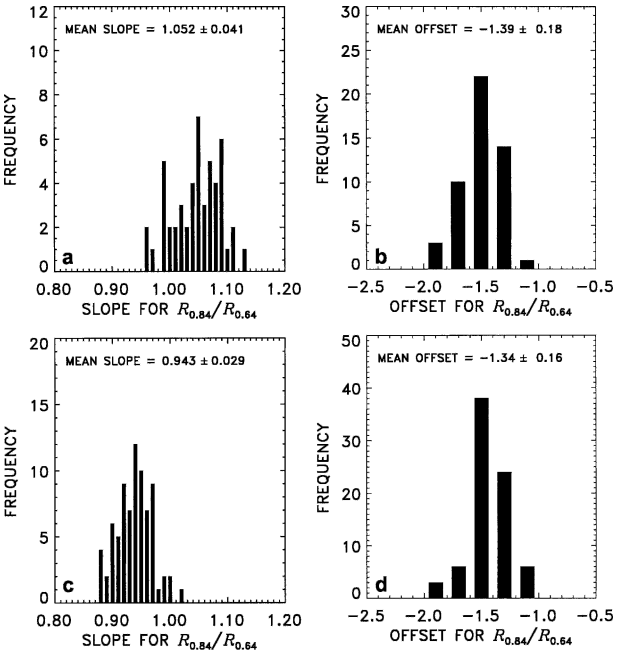

FIG. 11. Same as in Fig. 10 but for AVHRR on (a), (b) *NOAA-16* and (c), (d) *NOAA-17*.

varies from 0.77 to 0.87 for the regions and times covered by the AVHRR observations. Here a constant correction is used, recognizing that a constant value will lead to greater ranges in slopes and intercepts obtained with the AVHRR compared with those obtained with MODIS. Indeed, the slopes for the AVHRR instruments show a comparatively large range of variability. The MODIS observations lack this variability because, as discussed by Heidinger et al. (2002), the 0.84-μm channel on MODIS is much narrower than the channel on AVHRR and the center wavelength of the MODIS channel was chosen to avoid significant absorption by water vapor. Although large compared with the variability exhibited by MODIS, the variability exhibited by the AVHRR is sufficiently small to allow comparisons between the MODIS and AVHRR instruments. First, while the slopes obtained with the *NOAA-16* AVHRR are close to those obtained with the MODIS instruments, the discrepancies are sufficient to warrant further investigation. Second, the *NOAA-16* and *NOAA-17* AVHRRs produce distinctly different results for the slopes.

For several years, spatially uniform regions of the extensive ice sheets of Antarctica have been used to obtain calibration coefficients for the AVHRR 0.64- and 0.84-μm reflectances (Loeb 1997; Tahnk and Coakley 2001a,b and 2002b). These reflectances were tied to those of the *NOAA-9* AVHRR by Loeb (1997). The *NOAA-9* reflectances, in turn, were tied to other tar-

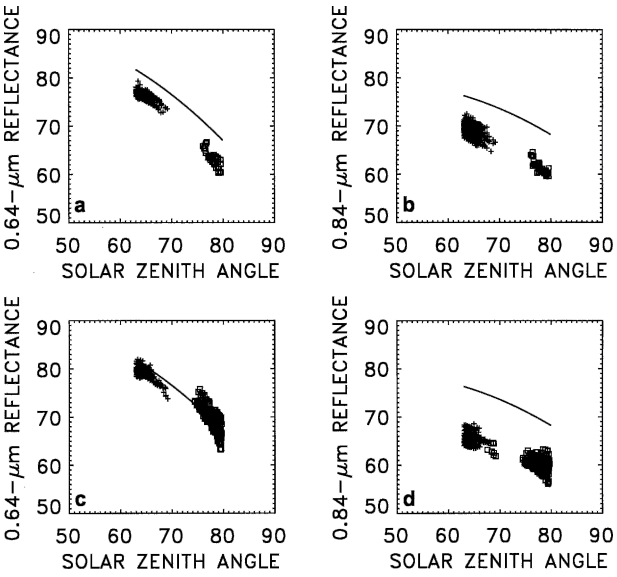

FIG. 12. The 0.64- and 0.84-μm nadir reflectances observed for spatially uniform regions of the Antarctic ice sheet during Dec 2002 for the AVHRR on (a), (b) *NOAA-16* and (c), (d) *NOAA-17*. Crosses indicate reflectances observed with the AVHRRs in their high-reflectance (low gain) modes and squares indicate reflectances observed in their low-reflectance (high gain) modes. The high-reflectance observations are generally obtained with the *NOAA-16* in its ascending branch of the orbit and the low-reflectance observations are obtained with the *NOAA-16* in its descending branch. For the *NOAA-17* the ascending branch yields the low-reflectance observations and the descending branch the high-reflectance observations. The curves in the figure are the reference reflectances for the ice sheets derived by Loeb (1997) from *NOAA-9* AVHRR observations.

gets for which there were independent observations of reflectances (Rao and Chen 1995). Figure 12 shows comparisons of the observed reflectances for December 2002 obtained with the AVHRRs on *NOAA-16* and *NOAA-17* and the reference reflectances derived by Loeb (1997) (solid curves). The procedures used to obtain the reflectances followed those outlined by Loeb (1997) with the following modifications: The index of spatial uniformity used here is given by

$$N = \frac{1}{4}\left(\frac{\sigma_{0.64}}{\Delta R_{0.64}} + \frac{\sigma_{0.84}}{\Delta R_{0.84}} + \frac{\sigma_{1.6}}{\Delta R_{1.6}} + \frac{\sigma_{11}}{\Delta T_{11}}\right) < 0.02, \tag{5}$$

where $\sigma_{0.64}$, $\sigma_{0.84}$, $\sigma_{1.6}$, and σ_{11} represent the standard deviations of the 0.64-, 0.84-, and 1.6-μm reflectances (%) and 11-μm brightness temperatures (K) for 17 $\times$ 17 arrays of the 4-km AVHRR Global Area Coverage (GAC) pixels having nadir angles less than 18°; and $\Delta R_{0.64} = 5\%$, $\Delta R_{0.84} = 5\%$, $\Delta R_{1.6} = 5\%$, and $\Delta T_{11} = 10$ K are the ranges of the 0.64-, 0.84-, and 1.6-μm reflectances and 11-μm brightness temperature observed for all such pixel arrays when viewing the extensive ice sheets in Antarctica during this period. The targets chosen for comparison with the *NOAA-9* reference reflectances lie in the region 72°–80°S, 90°–130°E. As for the sun-glint observations, the reflectances shown in Fig. 12 are given by (1) with an additional factor that accounts for the day-to-day changes in the Sun–Earth distance. In Fig. 12, the plus symbols indicate observations in which the AVHRRs were working in their high-reflectance (low gain) modes and the squares indicate observations obtained in the low-reflectance (high gain) modes. For the *NOAA-16*, the high-reflectance observations are obtained with the satellite in the ascending branch of the orbit over the Antarctic target and the low-reflectance observations are obtained with the satellite in the descending branch. For the *NOAA-17*, the branches of the orbits and the high and low-reflectance modes are reversed. For the *NOAA-16* AVHRR, the 0.64-μm gain for the low-reflectance mode is evidently 5% too low and the 0.84-μm gain for the low-reflectance mode is 12% too low. The reflectances for the high-reflectance modes are, within 2%, similarly low. In their comparison of the *Terra* MODIS and *NOAA-16* AVHRR reflectances, Heidinger et al. (2002) find the gain of the 0.64-μm channel in the low-reflectance (high gain) mode to be too low by 5%, consistent with the ice-sheet observations, and that for the 0.84-μm channel to be too low by 17%, within 5% of the current assessment. For the *NOAA-17* AVHRR, the 0.64-μm reflectance appears to need no correction. Any correction would be less than 2%. The 0.84-μm gain for the low-reflectance mode appears to be 15% too low. The gain of the high-reflectance mode is similarly low.

Figure 13 shows the slopes and intercepts derived for the 0.64- and 0.84-μm reflectances for the AVHRR on *NOAA-16* and *NOAA-17* with the calibration coefficients adjusted to agree with the *NOAA-9* reference reflectances for the Antarctic ice sheet. The slopes and intercepts for the two AVHRRs are now consistent with each other and also consistent with the slopes and intercepts for the two MODIS instruments. These results suggest that the discrepancies encountered for the *NOAA-16* and *NOAA-17* AVHRR 1.6-μm reflectances are probably due to differences in radiometric calibration and not to differences in the sensitivity of the instruments to polarization. With the gain of the *NOAA-16* AVHRR 0.64-μm channel adjusted, based on the ice sheet observations, the gain of the 1.6-μm channel, based on the sun-glint observations, is, in fact, accurate (within 1%). This result is reasonably consistent with the finding of Heidinger et al. (2002) that the *NOAA-16*

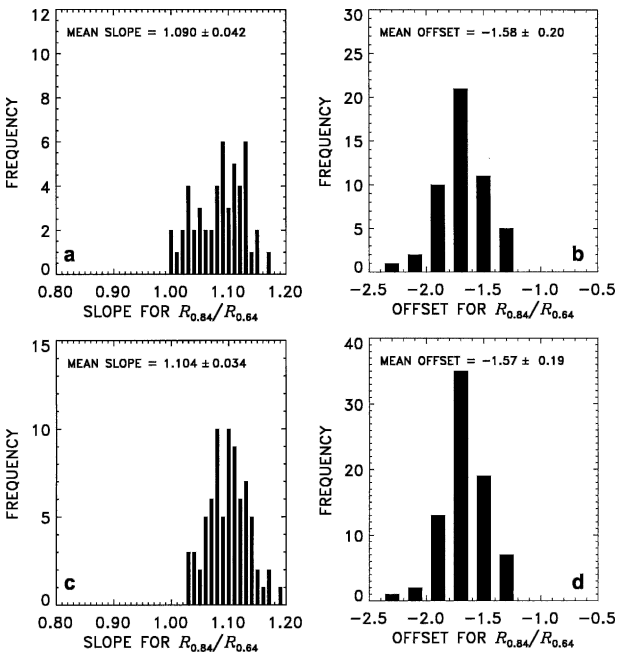

FIG. 13. Same as Fig. 10 but for AVHRR on (a), (b) *NOAA-16* and (c), (d) *NOAA-17* after corrections to the gains derived from observations of Antarctic ice sheets.

1.6-μm channel reads 6% too low for the low-reflectance (high gain) mode using the coefficients that they derived based on the MODIS–AVHRR comparisons.

5. Summary and conclusions

Simulations of reflected sunlight for regions of sun glint off water surfaces suggest that the reflectances might be used to assess the accuracies, in a relative sense, of the radiances at different wavelengths for imaging radiometers. The simulations show that for solar zenith angles less than 35° and for atmospheric windows, as long as the aerosol burden is relatively light and the aerosol is composed of large particles, as is the case for marine aerosols, the reflectances at different wavelengths are linearly related and the slopes and intercepts of the relationships are relatively insensitive to factors that strongly influence the reflectances themselves, such as surface wind speed and direction, atmospheric composition, and sun–surface–sensor geometry. That is, if the accuracy of the radiances at one wavelength is known, observations of sun glint can be used to check the calibration of the instrument at other wavelengths. The probable accuracy of these estimates is 5%. This strategy of using observations of sun glint to transfer the calibration of reflectances at one wavelength to those at other wavelengths was also recognized by Kaufman and Holben (1993). Even if the accuracies of the radiances at all wavelengths are unknown, observations of sun glint can be used to assess the stability of the instrument over time and determine whether the reflectances are related in a manner that is expected from theory. The approach is particularly suited for assessing the in-flight performance of aircraft-borne scanning radiometers such as the MCR and MAS.

Analyses of data from both the *Terra* and *Aqua* MODIS instruments, VIRS, which flew on the *TRMM* satellite, and the *NOAA-16* and *-17* AVHRRs were used to illustrate the method. Observations of sun glint were analyzed for the southern Indian Ocean, a region that is relatively free of aerosol and the prevailing aerosol is marine. The analysis of data from the two MODIS instruments yielded identical results for the 0.64-, 0.84-, 1.6-, and 2.1-μm reflectances. The results obtained with the MOCARAT Monte Carlo simulations were judged to be inaccurate owing to deficiencies in the representation of the aerosol optical properties. The model appeared to be more sensitive than the observations to the presence of aerosols at the visible wavelengths and less sensitive to the presence at near infrared wavelengths. Nevertheless, the MOCARAT simulations showed sensitivities to changes in wavelength, solar zenith angle, and aerosol loading that were qualitatively consistent with the observations.

Observations of sun glint for the 0.64- and 1.6-μm channels of VIRS were inconsistent with the MODIS results. Assuming that the VIRS 0.64-μm reflectances were correct, the results from the sun-glint observations indicated that the gain for the VIRS 1.6-μm channel was too low by approximately 9%, consistent with an assessment by Lyu and Barnes (2003), who estimated that the gain was too low by 8.2%, but inconsistent with the assessment by Minnis et al. (2002) who estimated that the gain was too low by 17%.

Prelaunch calibration coefficients were used to derive the 0.64- and 0.84-μm reflectances of the *NOAA-16* AVHRR and the 0.64-, 0.84-, and 1.6-μm reflectances of the *NOAA-17* AHVRR for December 2002. NOAA has updated calibration coefficients for *NOAA-16* AVHRR data collected after May 2003 and *NOAA-17* AVHRR data collected after May 2004. In the case of the *NOAA-16* AVHRR 1.6-μm channel, Heidinger et al. (2002) suggested that the prelaunch coefficients were inconsistent with the observed space count. For the *NOAA-16* 1.6-μm channel, the calibration coefficients used in this study were those derived by Heidinger et al. based on comparisons of *Terra* MODIS and *NOAA-16* AVHRR reflectances. Assuming the gains of the 0.64-μm AVHRR channels to be correct,

the sun-glint results indicated that the gain for the *NOAA-16* AVHRR 1.6-μm channel working in the low-reflectance (high gain) mode was too high by 6%, and that for the *NOAA-17* AVHRR was too low by 5%. For the *NOAA-16* AVHRR, Heidinger et al. (2002) reported that the 1.6-μm reflectances were too low by approximately 6%. As noted below, however, observations of the extensive ice sheets of Antarctica indicated that the gain of the *NOAA-16* AVHRR 0.64-μm channel was too low by 5% while that for the *NOAA-17* AVHRR was about right. Adjusting the gain of the *NOAA-16* 0.64-μm channel based on the ice sheet observations led to the estimate that the gain of the 1.6-μm channel was accurate (within 1%), which is reasonably consistent with the findings of Heidinger et al. (2002).

As a further test of using sun glint to determine the relative calibration of reflected radiances, reflectances at 0.64 and 0.84 μm were examined for the *Terra* and *Aqua* MODIS instruments and the *NOAA-16* and *-17* AVHRRs. The MODIS instruments produced 0.64–0.84-μm reflectance relationships that were consistent with each other; the AVHRR instruments produced relationships that were inconsistent with each other and inconsistent with the MODIS observations. New gains were derived for the 0.64- and 0.84-μm AVHRR channels using observations of extensive Antarctic ice sheets following procedures described by Loeb (1997). With the gains adjusted, based on the ice sheet observations, the 0.64- and 0.84-μm reflectances for regions of sun glint were found to be consistent with each other and consistent with the MODIS observations.

Acknowledgments. This work was supported in part by the NASA CERES Project through NAS1-98140 and in part by the NOAA Global Change Program through NA16GP2911. Part of this work was also performed while one of the authors (JAC) was a visitor in the NASA Goddard Earth Science and Technology Fellows Program at NASA's Goddard Space Flight Center. The hospitality, suggestions, and helpfulness of colleagues at Goddard were greatly appreciated. Comments by two anonymous reviewers substantially improved the presentation.

REFERENCES

Coakley, J. A., Jr., W. R. Tahnk, A. Jayaraman, P. K. Quinn, C. Devaux, and D. Tanré, 2002: Aerosol optical depths and direct radiative forcing for INDOEX derived from AVHRR: Theory. *J. Geophys. Res.,* **107,** 8009, doi:10.1029/2000JD000182.

Cox, C., and W. Munk, 1954: Measurement of the roughness of the sea surface from photographs of the sun's glitter. *J. Opt. Soc. Amer.,* **44,** 838–850.

Gao, B.-C., and A. F. H. Goetz, 1990: Column atmospheric water vapor and vegetation liquid water retrievals from airborne imaging spectrometer data. *J. Geophys. Res.,* **95,** 3549–3564.

Heidinger, A. K., C. Cao, and J. T. Sullivan, 2002: Using Moderate Resolution Imaging Spectrometer (MODIS) to calibrate advanced very high resolution radiometer reflectance channels. *J. Geophys. Res.,* **107,** 4702, doi:10.1029/2001JD002035.

Hess, M., P. Koepke, and I. Schult, 1998: Optical properties of aerosols and clouds: The software package OPAC. *Bull. Amer. Meteor. Soc.,* **79,** 831–844.

Kaufman, Y. J., and B. N. Holben, 1993: Calibration of the AVHRR visible and near-IR bands by atmospheric scattering, ocean glint, and desrt reflection. *Int. J. Remote Sens.,* **14,** 21–52.

——, J. V. Martins, L. A. Remer, M. R. Schoeberl, and M. A. Yamasoe, 2002: Satellite retrieval of aerosol absorption over the oceans using sunglint. *Geophys. Res. Lett.,* **29,** 1928, doi:10.1029/2002GL015403.

King, M. D., and Coauthors, 1996: Airborne scanning spectrometer for remote sensing of cloud, aerosol, water vapor, and surface properties. *J. Atmos. Oceanic Technol.,* **13,** 777–794.

——, and Coauthors, 2003: Cloud and aerosol properties, precipitable water, and profiles of temperature and water vapor from MODIS. *IEEE Trans. Geosci. Remote Sens.,* **41,** 442–458.

Liu, G., J. A. Curry, J. A. Haggerty, and Y. Fu, 2001: Retrieval and characterization of cloud liquid water path using airborne passive microwave data during INDOEX. *J. Geophys. Res.,* **106,** 28 719–28 730.

——, H. Shao, J. A. Coakley Jr., J. A. Curry, J. A. Haggerty, and M. A. Tschudi, 2003: Retrieval of cloud droplet size from visible and microwave radiometric measurements during INDOEX: Implication to aerosols' indirect radiative effect. *J. Geophys. Res.,* **108,** 4006, doi:10.1029/2001JD001395.

Loeb, N. G., 1997: In-flight calibration of NOAA AVHRR visible and near-IR bands over Greenland and Antarctica. *Int. J. Remote Sens.,* **18,** 477–490.

Lyu, C.-H., W. L. Barnes, and R. A. Barnes, 2000: First results from the on-orbit calibrations of the VIRS for TRMM. *J. Atmos. Oceanic Technol.,* **17,** 385–395.

——, and ——, 2003: Four years of TRMM/VIRS on-orbit calibrations and characterization using lunar models and data from *Terra*/MODIS. *J. Atmos. Oceanic Technol.,* **20,** 333–347.

Minnis, P., L. Nguyen, D. Doelling, D. Young, W. Miller, and D. Kratz, 2002: Rapid calibration of operational and research meteorological satellite imagers. Part I: Evaluation of research satellite visible channels as references. *J. Atmos. Oceanic Technol.,* **19,** 1233–1249.

Platnick, S., and Coauthors, 2000: The role of background cloud microphysics in the radiative formation of ship tracks. *J. Atmos. Sci.,* **57,** 2607–2624.

Ramanathan, V., and Coauthors, 2001: The Indian Ocean Experiment: An integrated assessment of the climate forcing and effects of the great Indo-Asian haze. *J. Geophys. Res.,* **106,** 28 371–28 399.

Rao, C. R. N., and J. Chen, 1995: Inter-satellite calibration of the visible and near-infrared channels of the advanced very high resolution radiometer on the *NOAA-7*, *-9*, and *-11* spacecraft. *Int. J. Remote Sens.,* **16,** 1931–1942.

Tahnk, W. R., and J. A. Coakley Jr., 2001a: Improved calibration coefficients for *NOAA-14* AVHRR visible and near-IR channels. *Int. J. Remote Sens.,* **22,** 1269–1283.

——, and ——, 2001b: Updated calibration coefficients for *NOAA-14* AVHRR channels 1 and 2. *Int. J. Remote Sens.,* **22,** 3053–3057.

——, and ——, 2002a: Aerosol optical depths and direct radiative forcing for INDOEX derived from AVHRR: Observations, January–March, 1996–2000. *J. Geophys. Res.,* **107,** 8010, doi:10.1029/2000JD000183.

——, and ——, 2002b: Improved calibration coefficients for *NOAA-12* and *NOAA-15* AVHRR visible and near-IR channels. *J. Atmos. Oceanic Technol.,* **19,** 1826–1833.

Vermote, E., and Y. J. Kaufman, 1995: Absolute calibration of AVHRR visible and near-infrared channels using ocean and cloud views. *Int. J. Remote Sens.,* **16,** 2317–2340.